JOC Article
pubs.acs.org/joc

Mechanism and Selectivity of Cinchona Alkaloid Catalyzed [1,3]-Shifts of Allylic Trichloroacetimidates

Nihan Çelebi-Ölçüm,[†] Viktorya Aviyente,[†] and K. N. Houk*,[‡]

[†]*Department of Chemistry, Boğaziçi University, Bebek, İstanbul 34342, Turkey, and* [‡]*Department of Chemistry and Biochemistry, University of California, Los Angeles, California 90095*

houk@chem.ucla.edu

Received May 26, 2009

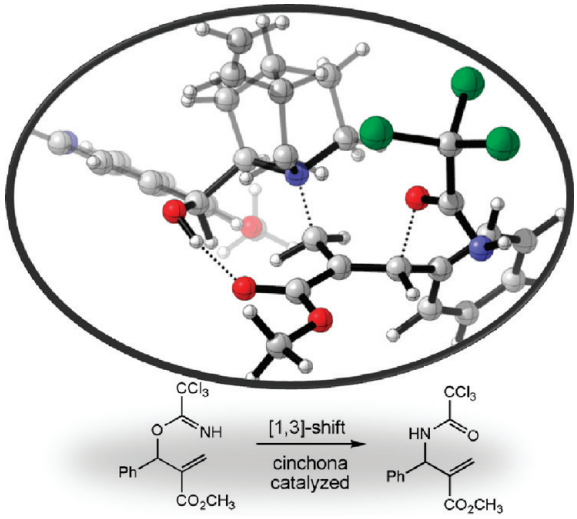

Density functional theory calculations were used to investigate the [3,3]- and [1,3]-shifts of *O*-allylic trichloroacetimidates in the presence of cinchona alkaloids. Thermal [1,3]- and [3,3]-rearrangements proceed through concerted pseudopericyclic transition states to give the corresponding rearranged products. [1,3]-Rearrangement is catalyzed via a double S_N2' mechanism in which *syn* addition of the nucleophile is exclusively preferred in both steps. The catalyzed mechanism is favored by a 6.3 kcal/mol free energy difference compared to the alternative [3,3]-rearrangement pathway. The fast-reacting enantiomer is predicted to be determined by the availability of the H-bonding interaction between the catalyst and the substrate.

Introduction

Cinchona alkaloids have found extensive use in organic chemistry as organocatalysts in asymmetric synthesis.[1−6] The success is also related to the fact that they can be tailored to catalyze specific reactions. Asymmetric primary amine derivatives of cinchona alkaloids are shown to be excellent activators of carbonyl compounds.[1] The 6′-hydroxy,[2] 9-thiourea,[3] and 6′-thiourea[4] derivatives have emerged as powerful bifunctional organocatalysts. Dimeric cinchona

(1) (a) Chen, Y.-C. *Synlett* **2008**, *13*, 1919–1930. (b) Zhou, J.; Wakchaure, V.; Kraft, P.; List, B. *Angew. Chem., Int. Ed.* **2008**, *47*, 7656–7658. (c) Singh, R. P.; Bartelson, K.; Wang, Y.; Su, H.; Lu, X.; Deng, L. *J. Am. Chem. Soc.* **2008**, *130*, 2422–2423. (d) Lu, X. J.; Liu, Y.; Sun, B.; Cindric, B.; Deng, L. *J. Am. Chem. Soc.* **2008**, *130*, 8134–8135. (e) Lu, X. J.; Deng, L. *Angew. Chem., Int. Ed.* **2008**, *47*, 7710–7713.

(2) (a) Marcelli, T.; van Maarseveen, J. H.; Hiemstra, H. *Angew. Chem., Int. Ed.* **2006**, *45*, 7496–7504. (b) Wang, B. M.; Wu, F.; Wang, Y.; Liu, X.; Deng, L. *J. Am. Chem. Soc.* **2007**, *129*, 768–769. (c) Wang, Y.; Li, H. M.; Wang, Y-Q.; Liu, L.; Foxman, B. M.; Deng, L. *J. Am. Chem. Soc.* **2007**, *129*, 6364–6365. (d) van Steenis, D. J. V. C.; Marcelli, T.; Lutz, M.; Spek, A. L.; van Maarseveen, J. H.; Hiemstra, H. *Adv. Synth. Catal.* **2007**, *349*, 281–286.

(3) (a) Connon, S. J. *Chem.—Eur. J.* **2006**, *12*, 5418–5427. (b) Song, J.; Wang, L.; Deng, L. *J. Am. Chem. Soc.* **2006**, *128*, 6048–6049. (c) Wang, Y. -Q.; Song, J.; Hong, R.; Li, H.; Deng, L. *J. Am. Chem. Soc.* **2006**, *128*, 8156–8157. (d) Song, J.; Shih, H,-W; Deng, L. *Org. Lett.* **2007**, *9*, 603–606. (e) Diner, P.; Nielsen, M.; Bertelsen, S.; Niess, B.; Jorgensen, K. A. *Chem. Commun.* **2007**, 3646–3648. (f) Aleman, J.; Milelli, A.; Cabrera, S.; Reyes, F; Jorgensen, K. A. *Chem.—Eur. J.* **2008**, *14*, 10958–10966.

(4) (a) Marcelli, T.; van der Haas, R. N. S.; van Maarseveen, J. H.; Hiemstra, H. *Angew. Chem., Int. Ed.* **2006**, *45*, 929–931. (b) Hammar, P.; Marcelli, T.; Hiemstra, H.; Himo, F. *Adv. Synth. Catal.* **2007**, *349*, 2537–2548. (c) Liu, Y.; Bingfeng, S.; Wang, B.; Wakem, M.; Deng, L. *J. Am. Chem. Soc.* **2009**, *131*, 418–419.

Published on Web 08/18/2009 DOI: 10.1021/jo901109s

SCHEME 1. [3,3]- and [1,3]-Sigmatropic Rearrangements of *O*-Allylic Trichloroacetimidates

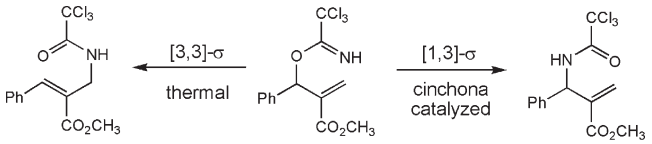

2 **1** **3**

alkaloids linked with various aromatic linkers provided very high enantioselectivities and are proposed to form enzyme like binding pockets for substrates.[5]

Despite the experimental reports on the use of cinchona alkaloid derivatives as organocatalysts, the origins of their enantioselective catalytic activity still remain unexplored. Elucidating the catalytic mechanisms of cinchona alkaloids is necessary to largely understand their catalytic efficiency.

In this study, we describe in detail the mechanism of the thermal and cinchona catalyzed rearrangements of allylic acetimidates yielding β-amino acid and allyl amine derivatives that are important building blocks found in many bioactive molecules. The experimental work by Jorgensen's group is an excellent example of cinchona catalysts,[6] and here we describe how their reactions occur.

Allylic trichloroacetimidate **1** undergoes either the well-known [3,3]-sigmatropic rearrangement (Overman rearrangement)[7] or the [1,3]-sigmatropic *O*- to *N*-rearrangement[8] to give the corresponding trichloroacetamides **2** and **3** (Scheme 1). The symmetry-forbidden [1,3]-rearranged product has been exclusively obtained in the presence of cinchona alkaloids, whereas the sterically hindered alkenes gave only the [3,3]-rearranged products.[6]

Computational Methodology

The geometries of reactants, transition states, and products were optimized using B3LYP/6-31G(d) with Gaussian 03.[9] Concerted and stepwise pathways for the thermal [1,3]-rearrangement were explored using UB3LYP/6-31G(d). Frequency calculations were used to verify the stationary points as minima or saddle points. The intrinsic reaction coordinate (IRC) method as implemented in Gaussian 03 was used to follow minimum energy paths from the transition states and to verify the nature of the reactants and products.[10] Single-point energies were computed with the M05-2X density functional method[11] and the 6-31+G(d,p) basis set. The M05-2X density functional method was chosen for its good performance for thermochemical kinetics and noncovalent interactions.[11,12] Solvent effects were taken into account via single-point calculations in a dielectric continuum representing toluene as the solvent. The conductor-like polarizable continuum model (CPCM) was applied using UAHF cavity model to compute the solvation free energies. The free energy (G) of a given structure in the solvent was calculated by

$$G = E_{\mathrm{gas}} + E_{\mathrm{zpe+thermal}} + \Delta G_{\mathrm{sol}} \quad (1)$$

where E_{gas} is the gas-phase electronic energy, $E_{\mathrm{zpe+thermal}}$ is the sum of the zero-point energy and the thermal and entropic contributions to the gas-phase energy at 298.15 K, and the last term ΔG_{sol} is the solvation free energy which can be described as the work required for transferring a system of a given geometry and standard state in vacuum to the solvent and contains both electrostatic and nonelectrostatic terms. All energetics reported throughout the text are given in terms of free energies in kcal/mol.

The topological analysis of the electron localization function (ELF),[13,14] was used to characterize the pericyclic and pseudopericyclic transition states using the TopMod suite of programs.[15,16] The characterization was based on the fluctuation analysis of the electron density at the cyclic reaction center.[17] In this procedure, covariance contributions to a bonding basin for the clockwise and counterclockwise directions determine the direction of larger electron fluctuation and are interpreted in terms of delocalization. The poor delocalization in pseudopericyclic reactions is evidenced by discontinuous charge distribution around the ring of forming and breaking bonds.

Potential energy surface (PES) scans were used to explore the conformational space of reactants, transition states and products. An initial systematic conformational search with 3 fold rotation around the single bonds was performed for the reactants and products using semiempirical PM3 methodology. The conformers within 3 kcal/mol energy range were then optimized using B3LYP/6-31G(d) for a more accurate description of the conformer distribution. A rigid PES scan was performed with B3LYP/6-31G(d) on the transition states using the dihedrals as specified in the results and discussion section. The low energy conformers of the transition states were later optimized using the same level of theory.

Results and Discussion

Conformational Flexibility of the Substrate. The conformational analysis of **1** has revealed the significant flexibility of the substrate with six conformers within 1.1 kcal/mol energy range (Figure 1). The energy differences between the *s-cis* and *s-trans* conformers are small (0.2−0.6 kcal/mol in the gas phase and 0.2−1.1 kcal/mol in toluene). The terminal alkene can either adopt an eclipsed conformation or a perpendicular arrangement with the C−O bond. The lowest energy conformer shows an eclipsed rearrangement of the terminal alkene and the C−O bond, but it is close in energy (0.6−0.8 kcal/mol in the gas phase and 0.8−1.0 kcal/mol in toluene) to the conformers with the perpendicular arrangement.

(5) (a) Tian, S.-K.; Chen, Y. G.; Hang, J. F.; Tang, L.; Mcdaid, P.; Deng, L. *Acc. Chem. Res.* **2004**, *37*, 621–631. (b) Corey, E. J.; Noe, M. C. *J. Am. Chem. Soc.* **1993**, *115*, 12579–12580. (c) Corey, E. J.; Noe, M. C.; Sarshar, S. *Tetrahedron Lett.* **1994**, *35*, 2861–2864. (d) Kolb, H. C.; Andersson, P. G.; Sharpless, K. B. *J. Am. Chem. Soc.* **1994**, *116*, 1278–1291. (e) Corey, E. J.; Noe, M. C. *J. Am. Chem. Soc.* **1996**, *118*, 319–329. (f) Corey, E. J.; Noe, M. C. *J. Am. Chem. Soc.* **1996**, *118*, 11038–11053.

(6) Kobbelgaard, S.; Brandes, S.; Jorgensen, K. A. *Chem.—Eur. J.* **2008**, *14*, 1464–1471.

(7) (a) Overman, L. E. *J. Am. Chem. Soc.* **1974**, *96*, 597–599. (b) Overman, L. E. *J. Am. Chem. Soc.* **1976**, *98*, 2901–2910.

(8) (a) Galeazzi, R.; Martelli, G; Orena, M.; Rinaldi, S. *Synthesis* **2004**, 2560–2566. (b) Hollis, T. K.; Overman, L. E. *J. Organomet. Chem.* **1999**, *576*, 290–299.

(9) Frisch, M. J. et al. *Gaussian 03, Revision D.01*; Gaussian, Inc.: Wallingford CT, 2004.

(10) (a) Gonzalez, C.; Schlegel, H. B. *J. Chem. Phys.* **1989**, *90*, 2154–2161. (b) Gonzalez, C.; Schlegel, H. B. *J. Phys. Chem.* **1990**, *94*, 5523–5527.

(11) Zhao, Y.; Schultz, N. E.; Truhlar, D. G. *J. Chem. Theory Comput.* **2006**, *2*, 364–382.

(12) Zhao, Y.; Truhlar, D. G. *J. Chem. Theory Comput.* **2007**, *3*, 289–300.

(13) (a) Savin, A.; Nesper, R.; Wengert, S.; Fässler, T. F. *Angew. Chem., Int. Ed.* **1997**, *36*, 1809–1832. (b) Marx, D.; Savin, A. *Angew. Chem., Int. Ed.* **1997**, *36*, 2077–2080. (c) Savin, A.; Becke, A. D.; Flad, J.; Nesper, R.; Preuss, H.; von Schnering, H. *Angew. Chem., Int. Ed.* **1991**, *30*, 409–412.

(14) Becke, A. D.; Edgecombe, K. E. *J. Chem. Phys.* **1990**, *92*, 5397–5403.

(15) Noury, S.; Krokidis, X.; Fuster, F.; Silvi, B. *TopMod Package*; Universite Pierre et Marie Curie: Paris, 1997.

(16) (a) Noury, S.; Krokidis, X.; Fuster, F.; Silvi, B. *Comput. Chem.* **1999**, *23*, 597–604. (b) Calatayud, M.; Andrés, J.; Beltrán, A.; Silvi, B. *Theor. Chem. Acc.* **2001**, *105*, 299–308. (c) Silvi, B. *J. Mol. Struct.* **2002**, *614*, 3–10. (d) Silvi, B. *J. Phys. Chem. A* **2003**, *107*, 3081–3085. (e) Silvi, B. *Phys. Chem. Chem. Phys.* **2004**, *6*, 256–260. (f) Matito, E.; Silvi, B.; Duran, M.; Solà, M. *J. Chem. Phys.* **2006**, *125*, 024301.

(17) Matito, E.; Poater, J.; Duran, M.; Solà, M. *ChemPhysChem* **2006**, *7*, 111–113.

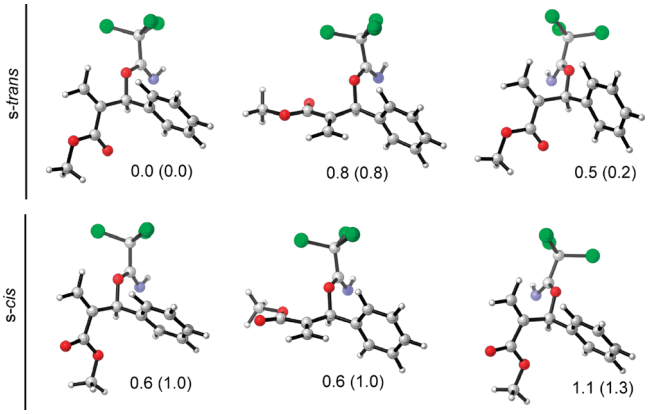

FIGURE 1. Low energy conformers of **1** and their relative free energies, ΔG_{gas} ($\Delta G_{toluene}$).

A thorough conformational search was performed on all transition states, whereas only the lowest energy conformers are discussed in the following sections. Other higher energy transition states are given in the Supporting Information.

Thermal Sigmatropic Rearrangement Pathways. The Overman rearrangement occurs via transition states **TS-[3,3]-1** and **TS-[3,3]-2**, with activation free energies of 27.3 and 27.7 kcal/mol, respectively (Figure 2a). The Overman rearrangement transition states are stabilized by 1.9 kcal/mol in toluene ($\Delta G^{\ddagger}_{toluene}$ **TS-[3,3]-1** = 25.4 kcal/mol and $\Delta G^{\ddagger}_{toluene}$ **TS-[3,3]-2** = 25.8 kcal/mol). **TS-[3,3]-1** and **TS-[3,3]-2** are very close in energy ($\Delta\Delta G^{\ddagger}_{gas} = \Delta\Delta G^{\ddagger}_{toluene} = 0.4$ kcal/mol) and differ in the *s-cis* and *s-trans* arrangements of the ester substituent. They can be described as pseudopericyclic[18] as evidenced by the disconnections in orbital overlap; orthogonal sets of orbitals meet, but there is no continuous overlap around the ring of forming and breaking bonds. The lack of cyclic "orbital" overlap is also apparent from the noncyclic pattern of electron fluctuations between the populations in the electron localization function (ELF) basins shown in Figure 2b. The ELF picture exhibits high localization over atoms N1, O3, and C5 while there are disconnections around the regions involving C2, C4, and C6. The process is concerted but asynchronous ($d_{C-O} = 1.71$ Å, $d_{C-N} = 1.97$ Å). The charge separation is 0.28e (0.25e in toluene). An equatorial arrangement of the phenyl ring leads to a destabilizing interaction between the ester and the phenyl groups; the transition states with the phenyl ring at an equatorial position are found to be more than 4.5 kcal/mol higher in energy (see the Supporting Information). The process is exothermic by 19.9 kcal/mol ($\Delta G_{toluene} = -21.5$ kcal/mol).

According to Woodward−Hoffmann rules, pericyclic transition structures are symmetry forbidden for [1,3]-sigmatropic rearrangements.[19] However, we found that the

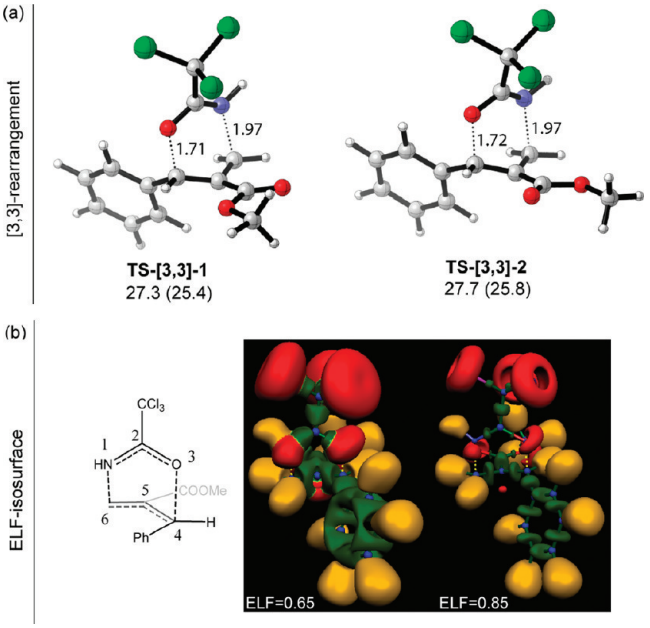

FIGURE 2. (a) Lowest energy transition states and their activation free energies, $\Delta G^{\ddagger}_{gas}$ ($\Delta G^{\ddagger}_{toluene}$), for the [3,3]-rearrangement and (b) the topology of the electron localization domain, represented by ELF = 0.65 and ELF = 0.85 isosurfaces for the [3,3]-rearrangement transition structures.

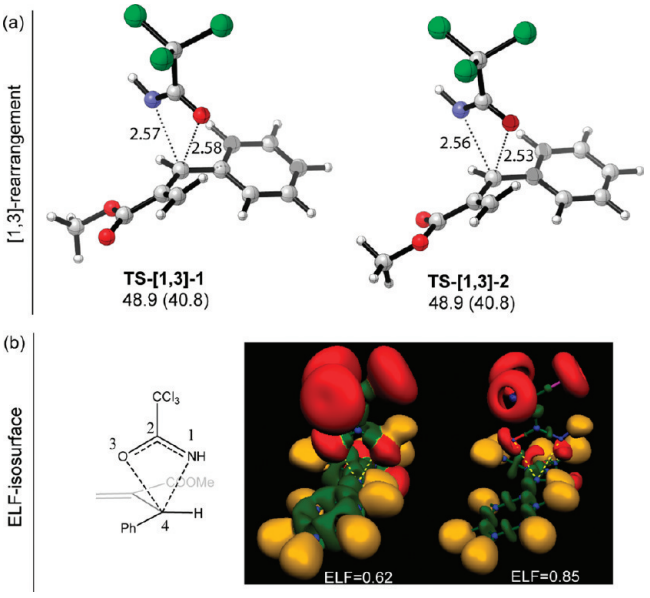

FIGURE 3. (a) Lowest energy transition states and their activation free energies, $\Delta G^{\ddagger}_{gas}$ ($\Delta G^{\ddagger}_{toluene}$), for the [1,3]-rearrangement and (b) the topology of the electron localization domain, represented by ELF = 0.62 and ELF = 0.85 isosurfaces for the [1,3]-rearrangement transition structures.

thermal [1,3]-rearrangement of **1** to **3** can occur via four membered pseudopericyclic transition states **TS-[1,3]-1** and **TS-[1,3]-2** (Figure 3a). The ELF picture (Figure 3b) shows electron depletion around C2 and C4, while the electrons are accumulated around N1 and O3. The electron distribution is not delocalized over the ring unlike a typical pericyclic reaction, but rather shows a localized picture with a

(18) (a) Ross, J. A.; Seiders, R. P.; Lemal, D. M. *J. Am. Chem. Soc.* **1976**, *98*, 4325–4327. (b) Birney, D. M.; Wagenseller, P. E. *J. Am. Chem. Soc.* **1994**, *116*, 6262–6270. (c) Birney, D. M. *J. Org. Chem.* **1996**, *61*, 243–251. (d) Birney, D. M.; Xu. X. L.; Ham, S. *Angew. Chem., Int. Ed.* **1999**, *38*, 189–193. (e) Birney, D. M. *J. Am. Chem. Soc.* **2000**, *122*, 10917–10925. (f) de Lera, A. R.; Alvarez, R.; Lecea, B.; Torrado, A.; Cossio, F. P. *Angew. Chem., Int. Ed.* **2001**, *40*, 557–561. (g) Shumway, W. W.; Dalley, N. K.; Birney, D. M. *J. Org. Chem.* **2001**, *66*, 5832–5839.

(19) (a) Woodward, R. B.; Hoffmann, R. *The Conservation of Orbital Symmetry*; Verlag Chemie: Weinheim, 1970. (b) Hoffmann, R.; Woodward, R. B. *Acc. Chem. Res.* **1968**, *1*, 17–22. (c) Hoffmann, R.; Woodward, R. B. *Angew. Chem., Int. Ed.* **1969**, *8*, 781–853.

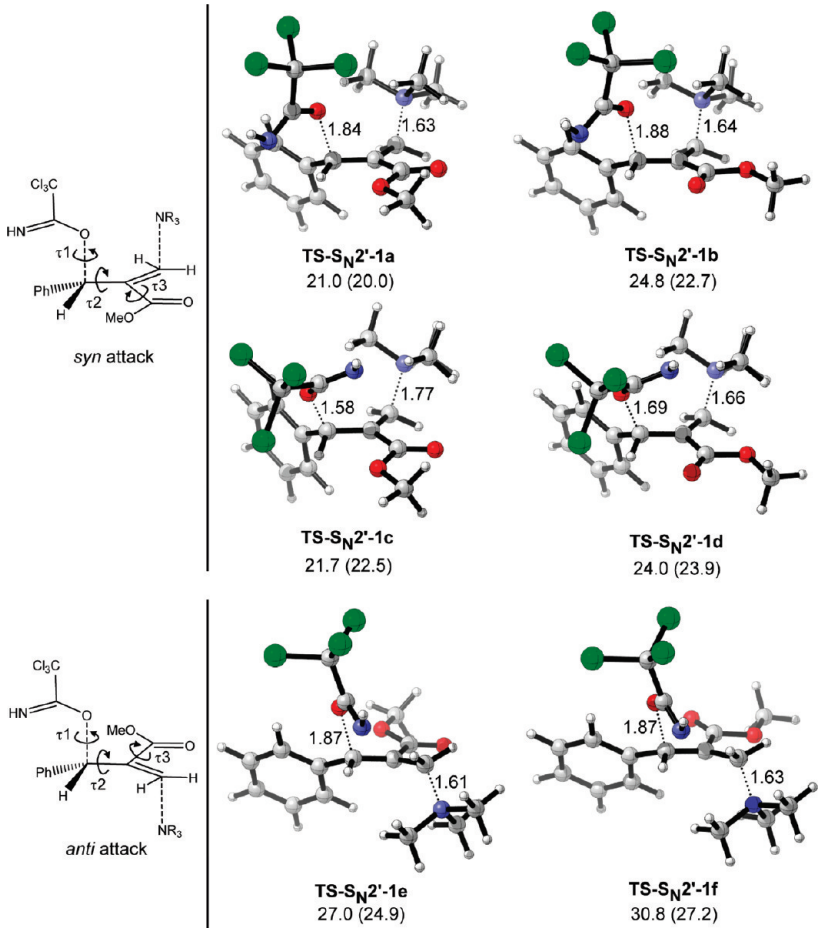

FIGURE 4. Lowest energy *syn* and *anti* transition states and their activation free energies, $\Delta G^{\ddagger}_{gas}$ ($\Delta G^{\ddagger}_{toluene}$), for the S_N2' reaction.

SCHEME 2. Proposed Mechanism for the Cinchona-Catalyzed [1,3]-Shifts

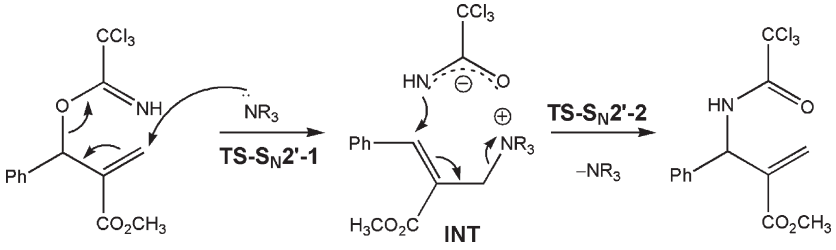

nonhomogeneous fluctuation scheme. Houk and Danishefsky have recently reported similar pseudopericyclic transition states for symmetry-forbidden [1,3]-acyl rearrangements.[20]

In contrast to the relatively easy thermal [3,3]-sigmatropic rearrangement process, 48.6 kcal/mol (40.8 kcal/mol in toluene) is required for the thermal [1,3]-rearrangement of **1** to **3**. **TS-[1,3]-1** is concerted and synchronous (d_{C-N} = 2.56 Å, d_{C-O} = 2.53 Å), but it is highly polar with a charge separation of 0.61e (0.86e in toluene). No evidence of diradical character in the transition state is found (S^2 = 0) even for unrestricted calculations, and the wave function is found to be stable. The *s-trans* arrangement of the ester, **TS-[1,3]-2**, is isoenergetic ($\Delta G^{\ddagger}_{gas}$ = 48.9 kcal/mol and $\Delta G^{\ddagger}_{toluene}$ = 40.8 kcal/mol) and also very similar in character to **TS-[1,3]-1**. We were not able to find any evidence for alternative stepwise pathways involving polar or radical pair intermediates. The homolytic or the heterolytic cleavage of the C−O bond of **1** is highly endothermic by 52.5 and 131.7 kcal/mol in the gas phase and 49.5 and 79.4 kcal/mol in toluene, respectively.

Mechanism of the Catalyzed Reaction. The proposed catalytic mechanism for [1,3]-shift of imidates to amides consists of a two-step S_N2' mechanism (Scheme 2). The attack of the nucleophilic amine is accompanied by loss of the trichloroacetimidate anion (**TS-S_N2'-1**). This establishes an ion-pair intermediate (**INT**). Subsequent attack of the nitrogen nucleophile of the anionic trichloroacetamide proceeds with the release of the catalyst in the second step (**TS-S_N2'-2**).

In order to reduce the computational cost, the mechanism was first investigated by using trimethylamine as the model catalyst. Both *syn* and *anti* attack of trimethylamine with respect to the trichloroacetimidate **1** were considered

(20) Jones, G. O; Li, X. C.; Hayden, A. E.; Houk, K. N.; Danishefsky, S. *J. Org. Lett.* **2008**, *10*, 4093–4096.

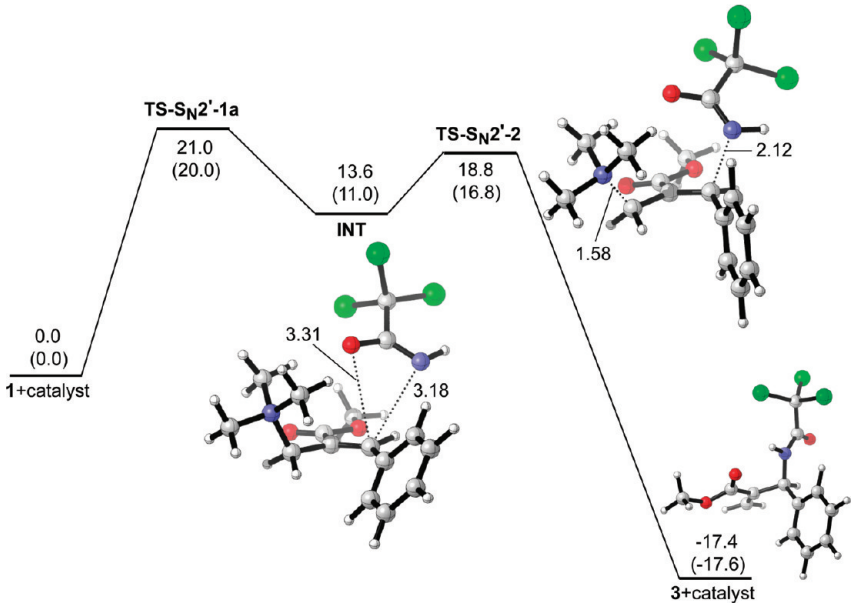

FIGURE 5. Free energy profile, ΔG_{gas} ($\Delta G_{toluene}$), for the trimethylamine-catalyzed [1,3]-shift of allylic trichloroacetimidate **1**.

(Figure 4). Due to the flexibility of the substrate, all transition state conformers obtained by rotation around $\tau 1$, $\tau 2$, and $\tau 3$ were analyzed.

The lowest energy s*yn* and *anti* transition state conformations are shown in Figure 4. **TS-S_N2'-1a** is the lowest energy transition state, with an activation free energy of 21.0 kcal/mol in the gas phase and 20.0 kcal/mol in toluene. The *anti* transition states, **TS-S_N2'-1e** and **TS-S_N2'-1f** are 6.0 and 9.8 kcal/mol higher in energy than **TS-S_N2'-1a**, respectively. Although the *anti* transition states **TS-S_N2'-1e** and **TS-S_N2'-1f** are better stabilized than their *syn* counterparts in toluene, their energies remain 4.9 and 7.2 kcal/mol higher than **TS-S_N2'-1a**, respectively. All other *anti* transition states have activation free energies above 30.8 kcal/mol. Houk and co-workers have also shown and discussed in detail the preference of the *syn* attack in S_N2' reactions.[21] **TS-S_N2'-1a** and **TS-S_N2'-1c** differ in $\tau 3$ resulting in 0.7 kcal/mol free energy difference in the gas phase and 2.5 kcal/mol in toluene ($\tau(C-C-O-C)_{\text{TS-SN2'-1a}} = -130.4°$, $\tau(C-C-O-C)_{\text{TS-SN2'-1c}} = -60.3°$). A notable preference for the s-*cis* conformation in the transition state is found, unlike that in the reactant (**TS-S_N2'-1a**/**TS-S_N2'-1b** ($\Delta\Delta G^{\ddagger}_{gas} = 3.8$ kcal/mol, $\Delta\Delta G^{\ddagger}_{toluene} = 2.7$ kcal/mol), **TS-S_N2'-1c**/**TS-S_N2'-1d** ($\Delta\Delta G^{\ddagger}_{gas} = 2.3$ kcal/mol, $\Delta\Delta G^{\ddagger}_{toluene} = 1.4$ kcal/mol) and **TS-S_N2'-1e**/**TS-S_N2'-1f** ($\Delta\Delta G^{\ddagger}_{gas} = 3.8$ kcal/mol, $\Delta\Delta G^{\ddagger}_{toluene} = 2.3$ kcal/mol)). The energy difference between **TS-S_N2'-1a** and the other alternative transition state conformations (see Figure 4) suggests that **TS-S_N2'-1a** controls the subsequent steps of the rearrangement process.

Figure 5 shows the reaction profile predicted from the IRC calculations. The IRC path connects **TS-S_N2'-1a** to the ion pair intermediate, **INT**, and to the reactant complex. **INT** is 7.4 kcal/mol (9.0 kcal/mol in toluene) downhill from **TS-S_N2'-1a**. The charge separation in the intermediate is found to be 0.85e in the gas phase and 0.95e in toluene. **INT** already shows a favorable arrangement for the subsequent attack of the nitrogen nucleophile of the anionic trichloroacetamide to the quaternary ammonium bound substrate. A small energy barrier of 5.2 kcal/mol (5.8 kcal/mol in toluene) to **TS-S_N2'-2** initiates the second S_N2' reaction. The IRC calculations have demonstrated that the addition−elimination process is concerted although very asynchronous with the forming and breaking C−N bond distances of 2.12 Å and 1.58 Å respectively. The total process is exothermic by 17.4 kcal/mol ($\Delta G_{toluene} = -17.6$ kcal/mol). We were not able to locate any transition state for an *anti* attack of trichloroacetamide anion in the second step.

The 6.3 kcal/mol free energy difference (5.4 kcal/mol in toluene) between the Overman rearrangement transition state **TS-[3,3]-1** and **TS-S_N2'-1a** explains the exclusive formation of the [1,3]-rearranged product in the presence of cinchona alkaloids, whereas high activation free energies rule out the possibility of a thermal [1,3]-rearrangement.

Reactions of Hindered *O*-Allylic Trichloroacetimidates. In contrast to **1**, the terminal alkene in acetimidate **4**, is sterically hindered, and therefore less prone to nucleophilic attack (Figure 6). Accordingly, **4** gave only the Overman rearranged acetamide and provided no evidence on nucleophilic catalysis.[6]

We found that [3,3]-rearrangement occurs via a concerted pseudopericyclic transition state with an activation free energy of 29.1 kcal/mol ($\Delta G^{\ddagger}_{toluene} = 27.8$ kcal.mol). The energetic penalty due to steric effects is much more significant for the competing S_N2' addition as expected. A 7.5 kcal/mol higher energy barrier (5.4 kcal/mol in toluene) for the addition of the amine nucleophile shows why the exclusive formation of the Overman product is observed experimentally. Unlike **1**, **4** failed to give the [1,3]-rearranged product upon attempted nucleophilic catalysis.

Selectivity of the Catalyzed Reaction. Scheme 3 summarizes the possible pathways for formation of the (*R*) and (*S*) products starting from a racemic mixture of allylic trichloroacetimidates. Our calculations with the model catalyst (NMe_3) have shown that the *syn* addition−elimination mechanism is highly preferred in both steps (see Figure 4). The formation of *anti* ion pairs and the possibility of a

(21) Houk, K. N.; Paddon-Row, M. N.; Rondan, N. G. *THEOCHEM* **1983**, *103*, 197–208.

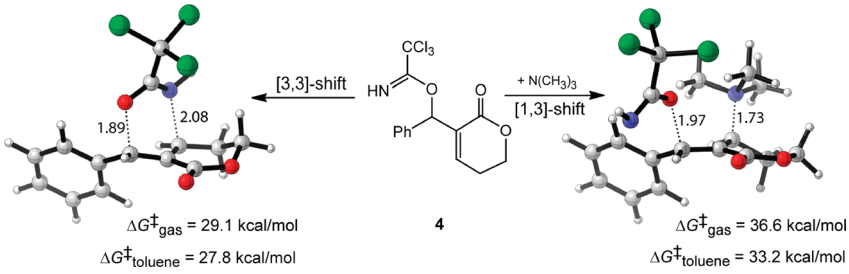

FIGURE 6. [3,3]- and [1,3]-rearrangements of hindered *O*-allylic trichloroacetimidates.

SCHEME 3. Possible Pathways of Cinchona-Catalyzed [1,3]-Shifts of Allylic Trichloroacetimidates

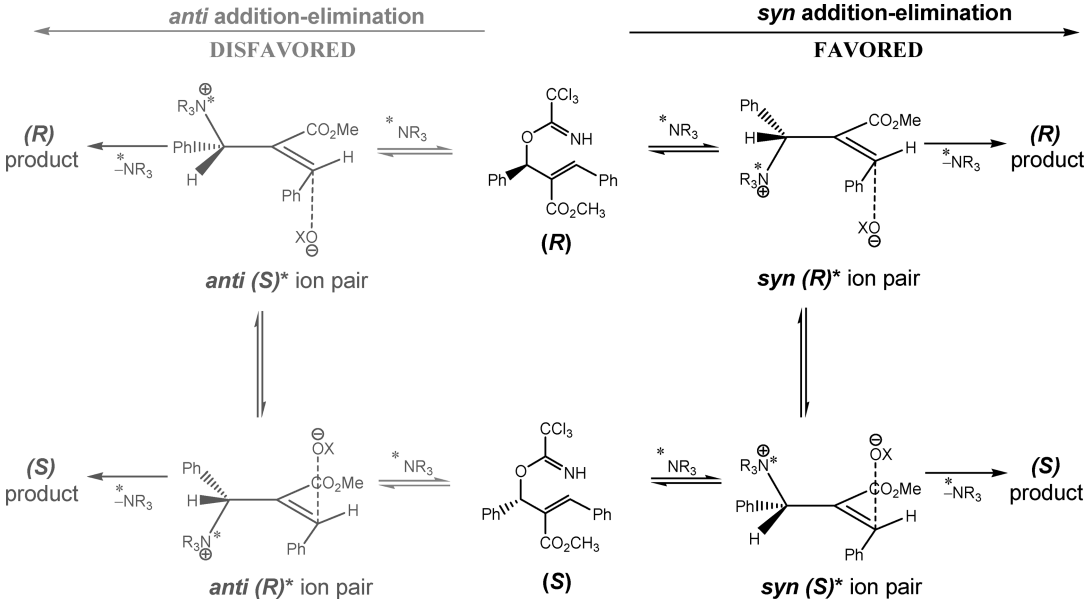

SCHEME 4. Stereoselectivities of Cinchona-Catalyzed [1,3]-Rearrangements

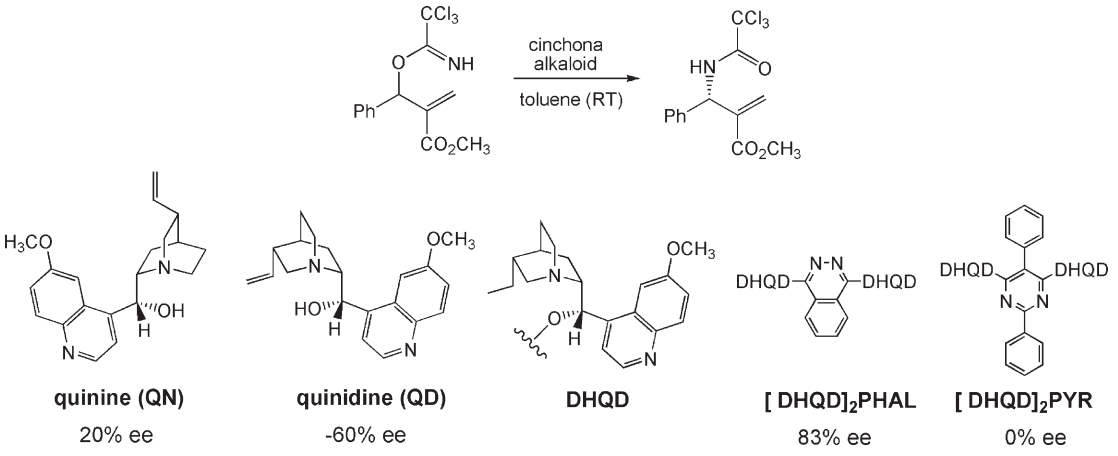

concomitant *anti* attack of another nucleophile are both strongly disfavored. These results suggest that the (*R*) and (*S*) enantiomers will react at different rates with the chiral amine nucleophile to form diastereomeric *syn* ion pairs in the first step. As the intermediate concentrations build up, the diastereomeric *syn* ion pairs will be engaged in a chemical equilibrium via a dissociation−recombination process. The selective *syn* addition of the nitrogen nucleophile of the anionic trichloroacetamide in the second step then designates the stereochemical outcome of the reaction. However, due to the high exothermicity of the reaction and the reversibility of the first step (see Figure 5), significant differences in the initial reaction rates may also affect the product distribution and the major product of the rearrangement process.

Cinchona-Catalyzed Reactions. Kobbelgaard et al.[6] have screened different cinchona alkaloids and have shown that the choice of the cinchona alkaloid has a remarkable impact

on the enantioselectivity of the reactions, with enantiomeric excess values ranging from 0% to 83% (Scheme 4). The selectivity of quinine (**QN**) is found to be very poor, whereas quinidine (**QD**) gave more promising enantioselectivities and favored the opposite enantiomer, as expected. The best results are obtained with the dimeric cinchona alkaloid (**DHQD)$_2$PHAL**, which resulted in enantiomeric excess values higher than 80%. However, a reversal of enantioselectivity occurred between quinidine and (**DHQD)$_2$PHAL**, although these two catalysts have identical stereochemistries of the binding site. More interestingly, dimeric cinchona alkaloids with different linkers such as (**DHQD)$_2$PYR** yielded a racemic mixture in toluene in contrast to the high enantioselectivities obtained with (**DHQD)$_2$PHAL**.

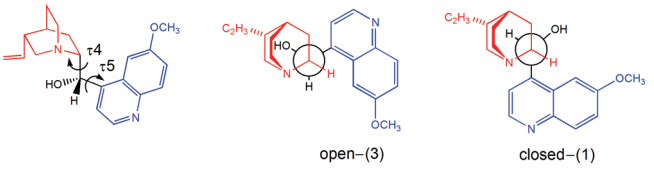

FIGURE 7. Open-(3) and closed-(1) conformations of quinidine, defined by the rotation around τ4 and τ5.

Quinidine- and quinine-catalyzed rearrangements of the racemic *O*-allyl trichloroacetimidate **1** were investigated here in order to elucidate the factors affecting the stereoselectivity of the real system. Previous experimental and computational studies have shown that cinchona alkaloids exist in solution as a mixture of rapidly interconverting conformers, and their conformational preferences have been extensively investigated.[22] These reports have shown that open-(3) and closed-(1) conformations, defined by the rotation around τ4 and τ5, dominate in most of the solvents usually favoring the open-(3) conformer (Figure 7). We, therefore, used open-(3) conformer of the catalyst in our calculations. We have chosen **TS-S$_N$2′-1a** and its enantiomer to serve as transition state templates. The dimensions of the conformational space are, thus, reduced with the help of the preceding knowledge on τ1−τ5.

Transition states (***R*)-TS-QD-I**, (***R*)-TS-QD-II** (Figure 8a), and (***S*)-TS-QD** (Figure 8b) were located by substituting the model catalyst with **QD-open-(3)** in the transition-state templates. The critical distances in all transition states are in close

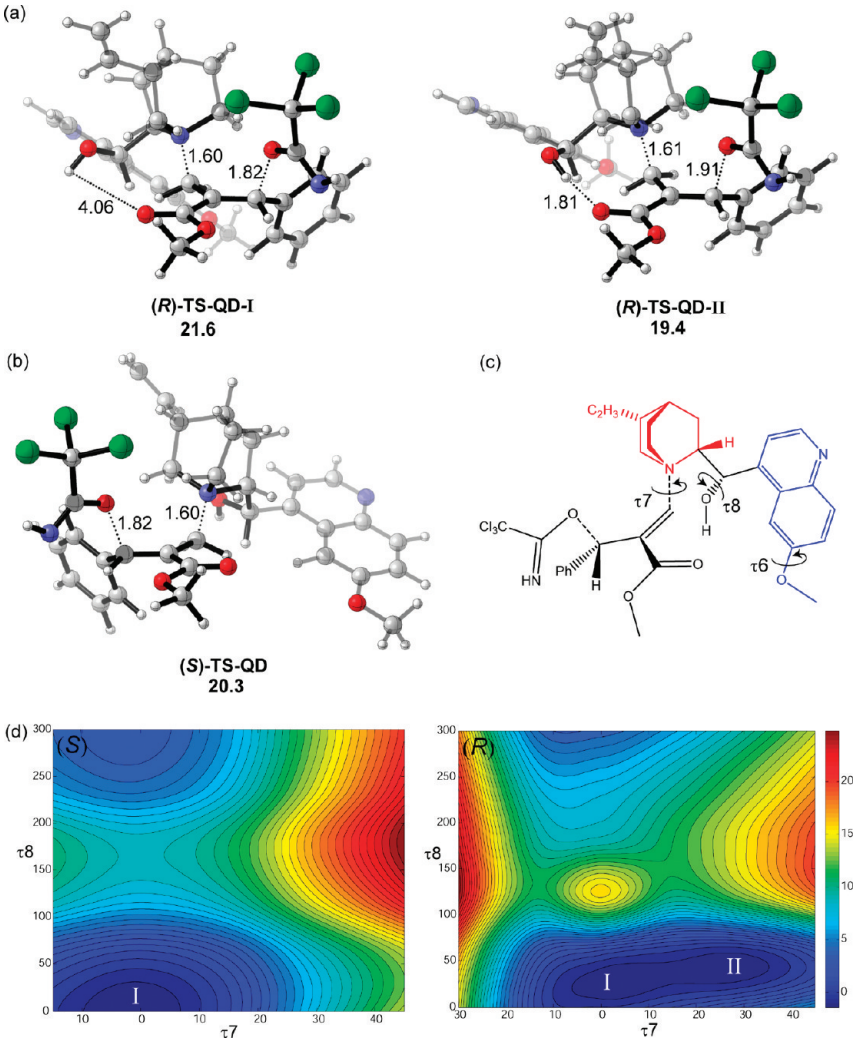

FIGURE 8. (a) Transition-state geometries and the activation free energies ($\Delta G^{\ddagger}_{gas}$) of the first S$_N$2′ step for the quinidine (**QD**)-catalyzed transformations of **1**-(*R*) and (b) **1**-(*S*). (c) Dihedrals used for the rigid potential energy surface scan. (d) Energy contour plots for the scan of τ7 versus τ8.

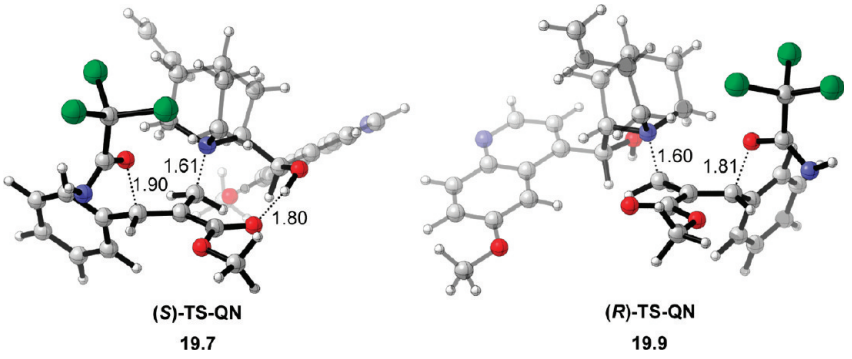

FIGURE 9. Transition-state geometries and the activation free energies ($\Delta G^{\ddagger}_{gas}$) of the first S_N2' step for the quinine (**QN**) catalyzed transformations of **1**-(*S*) and **1**-(*R*).

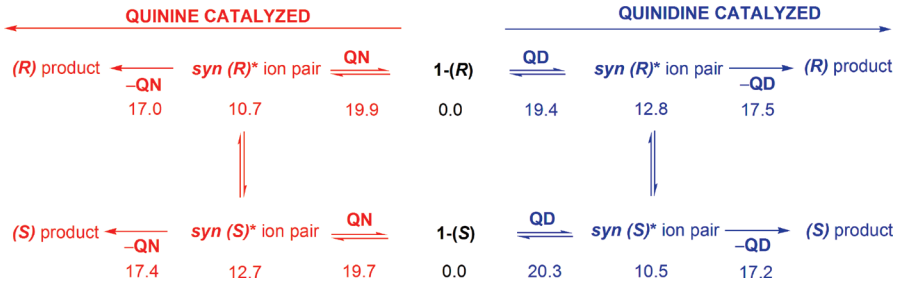

FIGURE 10. Energetics (ΔG_{gas}) of quinine (**QN**) and quinidine (**QD**) catalyzed [1,3]-rearrangements.

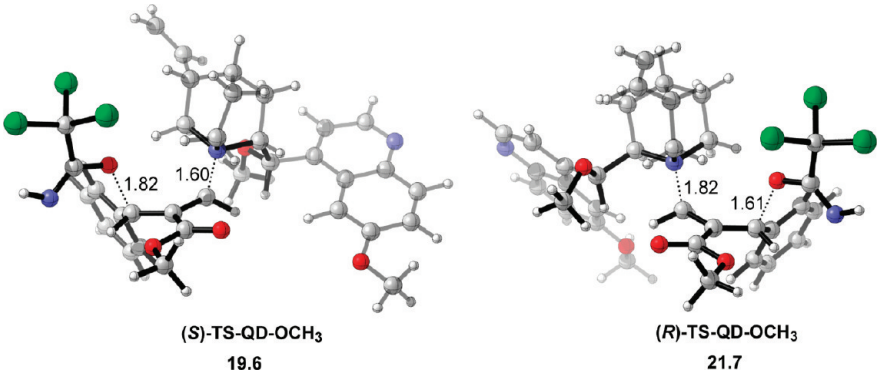

FIGURE 11. Transition-state geometries and the activation free energies ($\Delta G^{\ddagger}_{gas}$) of the first S_N2' step for transformations of **1**-(*S*) and **1**-(*R*) catalyzed by the quinidine methyl ether catalyst.

agreement with the model transition state **TS-S_N2′-1a**. (***R***)**-TS-QD-II** is 2.2 kcal/mol stabilized compared to (***R***)**-TS-QD-I** due to H-bonding interaction between the hydroxyl proton of the catalyst and the carbonyl oxygen on the substrate (1.81 Å). (***R***)**-TS-QD-II** is also 0.9 kcal/mol lower in energy than (***S***)**-TS-QD**. This clearly contrasts to the stability of (***S***)**-TS-QD** compared to (***R***)**-TS-QD-I** and suggests the importance of H-bonding interactions in determining the fast-reacting enantiomer. The lowest energy transition state (***R***)**-TS-QD-II** reveals the selective transformation of the *R* enantiomer in the first step.

The rigid PES scan on the transition-state geometries around the dihedrals τ6, τ7, and τ8 (Figure 8c) showed that there are no other low energy transition state alternatives. All geometries obtained from the rotation around τ6 are found to be higher in energy. The energy contour plots for the scan of τ7 versus τ8 are displayed in Figure 8d. The PES obtained for (***S***)**-TS-QD** has verified the existence of a single minimum corresponding to the located transition-state geometry for the transformation of the *S* enantiomer. Two alternative transition states for the *R* enantiomer are disclosed by two minima (**I** and **II**) on the PES corresponding to (***R***)**-TS-QD-I** and (***R***)**-TS-QD-II**.

Next, the reaction catalyzed by quinine was considered. In this case, (***S***)**-TS-QN** profits from the H-bonding interaction and only slightly favors the transformation of the *S* enantiomer by 0.2 kcal/mol compared to (***R***)**-TS-QN** (Figure 9). The relay of stereochemical information from the vinyl group seems negligible; quinine and quinidine catalyzed reactions have very similar activation energies.

The free energies for the complete processes are given in Figure 10. The geometries of ion-pair intermediates and

(22) (a) Dijkstra, G. D. H.; Kellogg, R. M.; Wynberg, H.; Svendsen, J. S.; Marko, I.; Sharpless, K. B. *J. Am. Chem. Soc.* **1989**, *111*, 8069–8076. (b) Dijkstra, G. D. H.; Kellogg, R. M.; Wynberg, H. *J. Org. Chem.* **1990**, *55*, 6121–6131. (c) Bürgi, T.; Baiker, A. *J. Am. Chem. Soc.* **1998**, *120*, 12920–12926. (d) Urakawa, A.; Meier, D. M.; Ruegger, H.; Baiker, A. *J. Phys. Chem. A* **2008**, *112*, 7250–7255.

transition states are very similar to **INT**, **TS-S_N2'-1a**, and **TS-S_N2'-2**. The fast-reacting enantiomer is determined by the H-bonding interaction between the catalyst and the substrate. Indeed, from the activation barriers of the first and the second S_N2' steps, the major product is predicted as the *R* enantiomer with quinidine and the *S* enantiomer with quinine, quinine giving lower enantioselectivity in agreement with the experimental results.[6]

The switch in the fast-reacting enantiomer due to hydrogen bonding has prompted us to verify our results by substituting the hydroxyl proton by a methyl group. Our results have demonstrated the preferential transformation of the *S* enantiomer in the first step as expected (Figure 11). These results qualitatively explain the experimentally observed change in the enantioselectivity of the reaction as the hydroxyl group on quinidine is modified by an aromatic linker to connect two dihydroquinidine units. However, the selectivity seems to rely on many other factors depending on the nature of the linkage and the solvent that are still to be explored.

Conclusion

The catalyzed [1,3]-rearrangement proceeds via a double S_N2' addition that is favored energetically compared to the competing pseudopericyclic Overman rearrangement pathway. Calculations with a model catalyst have suggested that *syn* addition−elimination is highly favored in both steps. Inclusion of the cinchona alkaloid catalysts has additionally revealed the importance of the H-bonding in accelerating the reaction. These results provide an initial but important understanding of the factors affecting the enantioselective catalytic activity of cinchona alkaloids as nucleophilic catalysts. However, the conformational space of the substrate and cinchona alkaloids is large and the selectivity seems to depend on many factors that are still to be explored.

Acknowledgment. We are grateful to the NIH-FIRCA project (R03TW007177), and the National Institute of General Medical Sciences, National Institutes of Health (GM36700 to K.N.H.), and the Boğaziçi University Research Fund (09M107). Computations were performed on the UCLA Academic Technology Services Hoffman Cluster and at the TUBITAK-ULAKBIM High Performance Computing Center.

Supporting Information Available: Cartesian coordinates, absolute energies, and complete ref 9. This material is available free of charge via the Internet at http://pubs.acs.org.